

Varying activity and the bursts properties of FRB 20240114A probed with GMRT down to 300 MHz

AJAY KUMAR ¹, YOGESH MAAN ¹ AND YASH BHUSARE ¹

¹*National Centre for Radio Astrophysics (NCRA - TIFR), Pune - 411007, India*

ABSTRACT

Repeating fast radio bursts can exhibit a wide range of burst repetition rates, from none to hundreds of bursts per hour. Here, we report the detection and characteristics of 57 bursts from the recently discovered FRB 20240114A, observed with GMRT in the frequency ranges 300-500 MHz and 550-750 MHz. Majority of the bursts show narrow emission-bandwidth with $\Delta\nu/\nu \sim$ around 10%. All of the bursts we detect are faint (<10 Jy ms), and thus probe the lower end of the energy distribution. We determine the rate function for FRB 20240114A at 400 MHz, and downward drift rates at 400 and 650 MHz, and discuss our measurements in the context of the repeating FRB population. We observe sudden variations in the burst activity of FRB 20240114A over time. Our data as well as the other publicly available information on other observations of FRB 20240114A so far, there is an indication that FRB 20240114A potentially exhibit a chromaticity in its burst activity. While the burst properties of FRB 20240114A are similar to other repeating FRBs, the frequency-dependent activity, if established, could provide crucial clues to the origin of repeating FRBs. We also place the most stringent 5σ upper limits of $600 \mu\text{Jy}$ and $89 \mu\text{Jy}$ on any persistent radio source (PRS) associated with FRB 20240114A at 400 MHz and 650 MHz, respectively, and compare these with the luminosity of the known PRSs associated with FRB121102A and FRB190520B.

Keywords: Fast Radio Bursts (2008) — FRBs (2008) — Radio Transients (1868)

1. INTRODUCTION

Fast radio bursts (FRB) are coherent bright radio flashes of cosmological origin with duration ranging from a few micro to several milliseconds. Their exceptional high dispersion measure (DM) along the line of sight can not be explained by the Galactic electron content, thus predicting their extragalactic origin. This is now confirmed with several repeating FRBs localized to a variety of galaxies (Chatterjee et al. 2017a; Bannister et al. 2019; Marcote et al. 2020; Bhandari et al. 2020; Heintz et al. 2020). The origin and emission mechanism of FRBs still remain an open question. Currently there are ~ 800 published FRBs, of which some are repeating in nature. Discovery of the first repeating FRB, FRB 20121102A (Spitler et al. 2014), ruled out cata-

clysmic events as the source for repeating FRBs. Currently there are close to sixty repeaters known¹ but only a few are known to be extremely active occasionally. A few repeating FRBs show periodicity in their activity, e.g., FRB180916 and FRB121102A exhibit periodicities of 16.35 and about 157 days (Chime/Frb Collaboration et al. 2020; Rajwade et al. 2020a). Some FRBs also show very high bursts rates (>100 bursts/hr) occasionally, e.g., FRB201124A and FRB220912A (Zhou et al. 2022; Feng et al. 2023). Several repeaters have been followed up or monitored over a long duration of time and their properties very well studied but we still we do not have source models that can explain all their observed properties. Discovery of highly active repeaters can provide more detailed insights into the observed spectro-temporal properties like narrow-band emission-behaviour and downward drifting pattern that has been seen across all repeaters.

akumar@ncra.tifr.res.in

ymaan@ncra.tifr.res.in

ybhusare@ncra.tifr.res.in

¹ <https://www.chime-frb.ca/repeaters>

Recently CHIME reported a discovery of a highly active repeating FRB 20240114A (Shin & CHIME/FRB Collaboration 2024). Starting on January 14, 2024, CHIME/FRB detected three bursts from FRB 20240114A within a week, and at a DM of 527.7 pc cm^{-3} consistent for all the bursts. The CHIME/FRB daily exposure time of only 4 minutes for this source suggested that a high burst rate above the fluence thresholds of $\sim 1 \text{ Jy ms}$ (Shin & CHIME/FRB Collaboration 2024). There were prompt follow ups from various telescopes including Parkes, FAST and ours using various frequency bands of GMRT (300-500 MHz, 550-750 MHz and 1060-1460 MHz), which confirmed the high activity of FRB 20240114A (Uttarkar et al. 2024; Pellicciari et al. 2024a; Kumar et al. 2024).

Subsequently, FRB was localized to an arc-second precision by the MeerKAT telescope (Tian et al. 2024). Following this localization, we focused on low frequency study of FRB 20240114A using band-3 (300-500 MHz) of uGMRT. One of our observations was on 05 March when there was a burst storm as reported by FAST (Zhang et al. 2024a). Since then, several other detections have been reported from P-band to frequencies up to 6 GHz (Uttarkar et al. 2024; Ould-Boukattine et al. 2024a; Zhang et al. 2024b; Pellicciari et al. 2024a; Kumar et al. 2024; Panda et al. 2024a; Zhang et al. 2024a; Pellicciari et al. 2024b; Snelders et al. 2024; Tian et al. 2024; Ould-Boukattine et al. 2024b; Hewitt et al. 2024; Joshi et al. 2024; Shin & CHIME/FRB Collaboration 2024).

Low frequency study of active repeating FRBs provide constraints to various proposed progenitors models for repeating FRBs (e.g., Pastor-Marazuela et al. 2021a). They also help in studying some of the propagation effects and the underlying emission mechanism (Gopinath et al. 2023; Pleunis et al. 2021a). Narrow-band behaviour has been reported for repeating FRBs (Kumar et al. 2021a) and it has been also been linked to giant pulses from pulsars and magnetars (Thulasiram & Lin 2021; Maan et al. 2019a). Magnetars appear to be the plausible originators of some of the repeating FRBs, especially since the detection of a millisecond duration burst from the Galactic magnetar SGR 1935+2154 with an energy comparable to the faintest FRBs (CHIME/FRB Collaboration et al. 2020; Bochenek et al. 2020). The low-frequency observations further help in studying the wide-band spectral behaviour of FRBs and probe any potential chromatic evolution of the activity (Pastor-Marazuela et al. 2021a; Pleunis et al. 2021a).

In this paper, we report detection of 57 bursts at low radio frequencies and narrow-band emission from FRB 20240114A. We present the results from the observations

done in band-4 (550-750 MHz), band-3 (300-500 MHz) and band-5 (1060-1460 MHz) of the upgraded GMRT. We describe the observation and the search procedure in section 2, the rate function at 400 MHz and extreme narrow-band emission in section 3. Burst properties are detailed in section 3, we discuss the implications of our results for observed properties of the repeating FRBs and their proposed formation channels in section 5. Finally, we conclude in the Section 6.

2. OBSERVATIONS AND SEARCH PROCEDURE

Following a possible high level of activity from the repeating FRB 20240114A reported by (Shin & CHIME/FRB Collaboration 2024), we conducted prompt follow-up observations using the upgraded giant metrewave radio telescope (uGMRT; Gupta et al. 2017). We utilized the wide frequency coverage of uGMRT, spanning 300 MHz to 1460 MHz. Specifically, we observed the source for 114 minutes in band-4 (550–750 MHz) on 01 February 2023, 104 and 71 minutes in band-3 (300–500 MHz) on 08 and 12 February 2023, respectively, and 65 minutes in band-5 (1060–1460 MHz) on 13 February 2023. These observations utilized recording in three different beams: phased-array (PA) beam and the PA spectral voltage (PASV; spectral voltage recording at the Nyquist rate) beam utilizing antennas in compact configuration, and the incoherent array (IA) beam. We simultaneously recorded the interferometric visibility data with a sampling time of 0.67 seconds to potentially localize the source within a few arcseconds using a burst with adequate signal-to-noise ratio (S/N). On 12 Feb 2024, we formed four PA beams with different antenna configurations to potentially obtain a localization better than the position known at that time (about 1.5 arcmin uncertainty, Shin & CHIME/FRB Collaboration 2024).

Sensitivity of our above observations was limited as the actual source was about 1.2 arcmin away from the best estimated position at that time. After FRB 20240114A was localized by MeerKAT to RA = $21^{\text{h}}27^{\text{m}}39.83^{\text{s}}$ and Dec = $04^{\text{d}}19^{\text{m}}46.02^{\text{s}}$ (Tian et al. 2024) with about an arcsec precision, we followed it for six more hours at band-3, now utilizing the full sensitivity of the PA beams. Observations were done in three epochs on 05, 08, and 24 March 2024 with the cumulative on-source times of 55, 85, and 75 minutes, respectively. More recently, we also had two observations at band-4, on 29 May 2024 and 15 June 2024, with cumulative on-source times of 126 minutes in each. In each of these sessions, we recorded the PA beam with 4096 frequency channels and a time resolution of $655 \mu\text{s}$. PASV data were also recorded simultaneously, which were co-

herently dedispersed and converted to filterbank format with 1024 frequency channels and a time resolution of $81.92 \mu\text{s}$ in the offline processing.

In all the above sessions, we use the following reduction and search procedures. The raw data are recorded with 16384, 4096, 4096 frequency channels and with time resolutions of $655.36 \mu\text{s}$, $327.28 \mu\text{s}$, $163.84 \mu\text{s}$ in bands 3, 4 and 5, respectively. For the band-3 observations conducted in March, we convert the PASV data to filterbank format with a sampling time of $81.92 \mu\text{s}$ and 1024 frequency channels. All these raw data are passed through a number of RFI excision rounds as follows. First, RFIClean² (Maan et al. 2021) is used to mitigate periodic, broadband and spiky RFI as well as convert the data to SIGPROC filterbank format. Subsequently, dedispersion from SIGPROC is used to subband the data to 1024 frequency channels, followed by one more round of RFI mitigation using RFIClean. Finally, we execute `rfifind` from PRESTO (Ransom 2011) to compute a mask of further identified RFI-contaminated segments in the data.

We use `prepdata` from PRESTO to dedisperse over a range of DMs from 522 to 532 pc cm^{-3} , with a step of 0.1 pc cm^{-3} for band-3 and 0.2 pc cm^{-3} for band-4. The dedispersed time-series are searched for single pulses using `single_pulse_search.py` above S/N of 7 and with a maximum boxcar width of 0.5 sec. The candidates are clustered in arrival times and DM, and then the candidate corresponding to highest S/N in the individual clusters is verified visually using the waterfall plot prepared using the package `your` (Aggarwal et al. 2020).

For the sub-band search, we divide the 200 MHz bandwidth in band-4 as well as band-3 into 7 sub-bands. Each sub-band has a bandwidth of 50 MHz and their the central frequency varies from 325 to 475 MHz for band-3, and 575 to 725 MHz for band-4, in steps of 25 MHz. Thus, there is 50% overlap between successive sub-bands. The dedispersion for these sub-bands is realized by ignoring the frequency channels not desired for a particular sub-band. The remaining part of the search procedure is same as described earlier.

In the Figure 1 top panel, we show the detection and non-detection of bursts reported at different frequencies in four different ranges: 0.3 to 0.8 GHz, 0.8 to 2.2 GHz, 2.2 to 4 GHz and 4 to 6 GHz, over the duration from 14/01/24 to 09/05/24 roughly every ten days. Here, we use the limited information that is available from various Atels published during this period.

3. BURST ANALYSIS AND RESULTS

We detected 10 bursts from our band-3 and band-4 observations conducted before the source well localized (Tian et al. 2024). In these observations, the pointing center was offset from the actual source position by 1.2 arcminutes (Tian et al. 2024). Of the 10 bursts, 5 were detected in band-4 (550-750 MHz) with an on-source time of 114 minutes, but only in the IA beam indicating that the actual source position was offset by more than the PA beam width (1.1 arcmin). Additionally, we detected 5 bursts in band-3 in the PA beam despite the offset as the PA beam width was adequately larger at these lower frequencies. We corrected the measured fluences for these observations to account for the offset from the actual position. Consequently, we estimate the burst rate to be 2.6 hr^{-1} at 650 MHz above the fluence of 0.64 Jy ms, seven days after CHIME detected two bright bursts from FRB 20240114A (Shin & CHIME/FRB Collaboration 2024).

From our later observations in March 2024, conducted in band-3 (300-500 MHz) and now using the improved position estimate, we detected significant activity. On 5th March 2024, approximately 3 hours and 15 minutes after a FAST observation wherein a sudden extremely high activity (burst rate of 500 hr^{-1} above a fluence of 0.015 Jy ms Zhang et al. 2024a) was noticed, we detected about 27 bursts within 52 minutes, implying a burst rate of 31 hr^{-1} at a fluence threshold of 0.2 Jy ms. The rate varies significantly over short durations, as we detected only 5 bursts on 8th March 2024, and all within the first 10 minutes out of nearly 75 minutes of the total on-source time. The rate seemed to have decreased by a factor of 8 in three days. Also, there were several bursts reported at P and L-band after this session (Snelders et al. 2024; Ould-Boukattine et al. 2024b; Hewitt et al. 2024; Joshi et al. 2024) implying varying activity level. On 24th March, we detected 15 bursts from an on-source time of 75 minutes. We did not detect any burst from our band-4 session on 29 May 2024.

In total, we detected 52 bursts in band-3 (300-500 MHz) and 5 bursts in band-4 (550-750 MHz). Some of these bursts exhibit a downward drifting pattern and majority are narrow-band in nature, as shown in Figure 1. Many bursts are primarily centered in the higher part of band-3, i.e., above 400 MHz, as evident from Figure 2, however, it is most likely caused by typical more RFI contamination in the central and lower half of band-3.

3.1. Rate Function

For each of the bursts, we use the filterbank files and the RFI mask described in Section 2, to prepare a time

² <https://github.com/ymaan4/RFIClean>

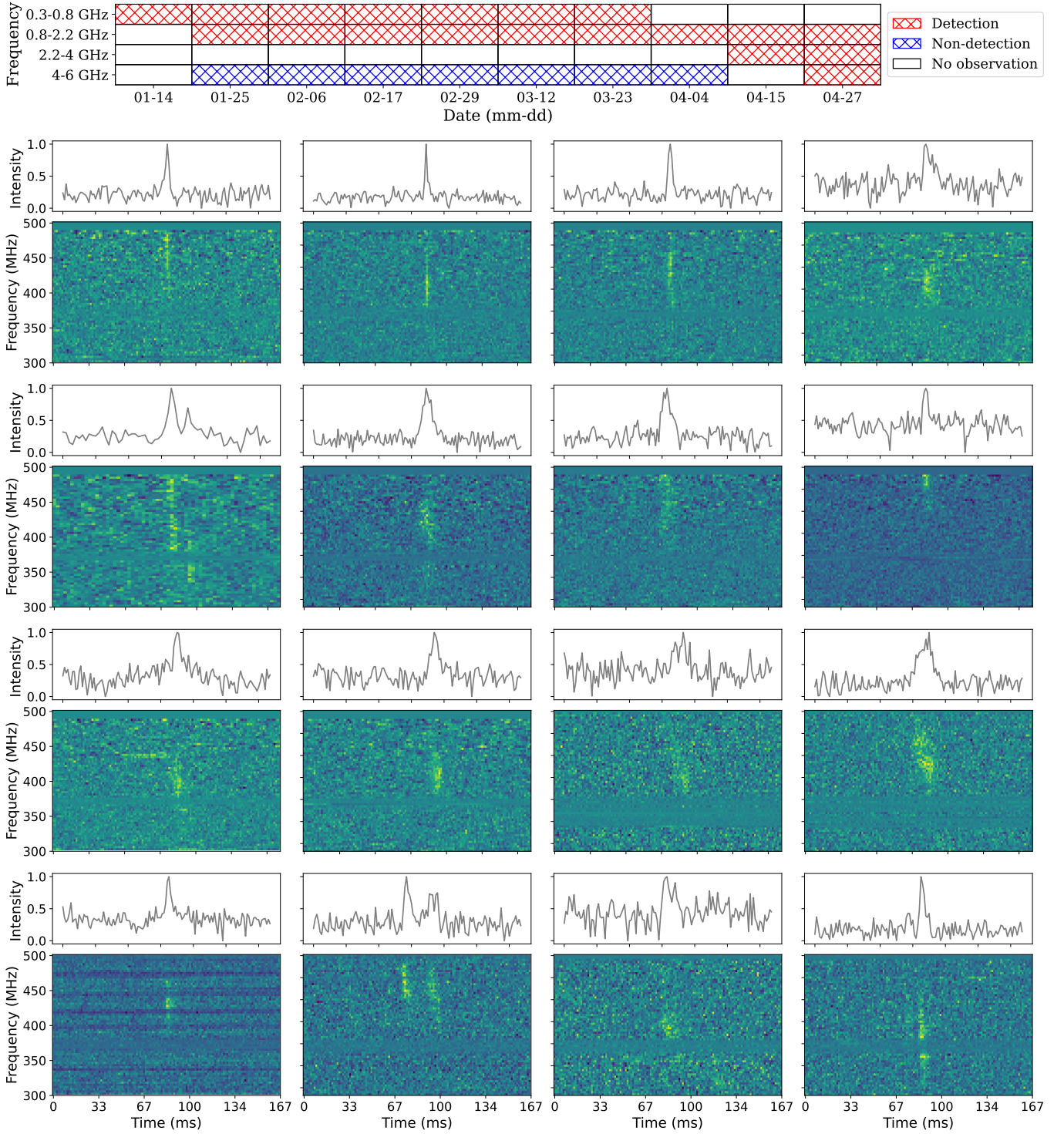


Figure 1. *Top:* A summary of the observations and detection/non-detection of bursts reported at different frequencies, ranging from P-band to C-band, over the duration from 14/01/24 to 09/05/24. The data used here are from various Atels published between 28/01/24 and 09/05/24 (Shin & CHIME/FRB Collaboration 2024; Uttarkar et al. 2024; Ould-Boukattine et al. 2024a; Zhang et al. 2024b; Pellicciari et al. 2024a; Tian et al. 2024; Kumar et al. 2024; Panda et al. 2024a; Zhang et al. 2024a; Snelders et al. 2024; Pellicciari et al. 2024b; Ould-Boukattine et al. 2024b; Hewitt et al. 2024; Joshi et al. 2024; Limaye & Spitler 2024). *Bottom:* Dynamic Spectra and time series of some of the bursts detected at band-3 (300-500 MHz).

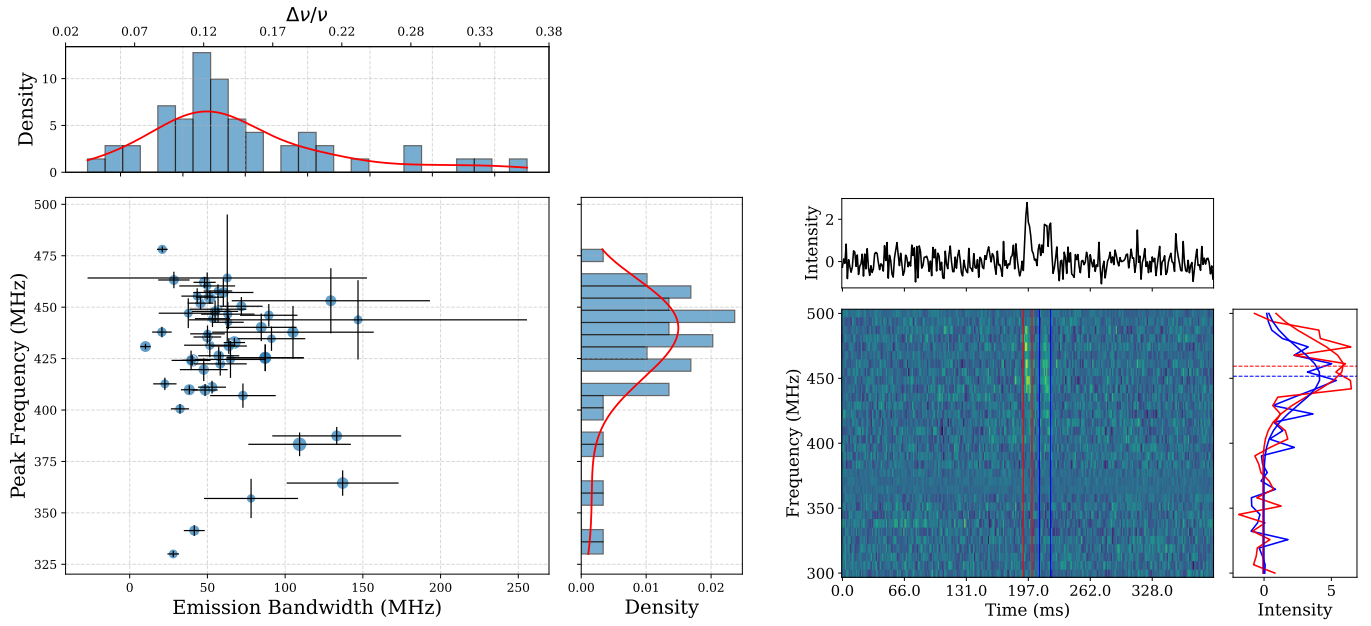


Figure 2. *Left:* Variation of the measured peak frequency with the emission bandwidth. The red line denotes the Gaussian kernel density function for the distribution of the fractional emission bandwidth ($\Delta\nu/\nu$) at top and for the peak frequency at right. *Right:* Example of a burst showing downward drifting pattern and Gaussian fits to the spectra for each component. In the right panel, spectra obtained from averaging along time axis for the regions marked in left panel under each component are shown. The red and green horizontal lines indicate the peak frequency for each of the component.

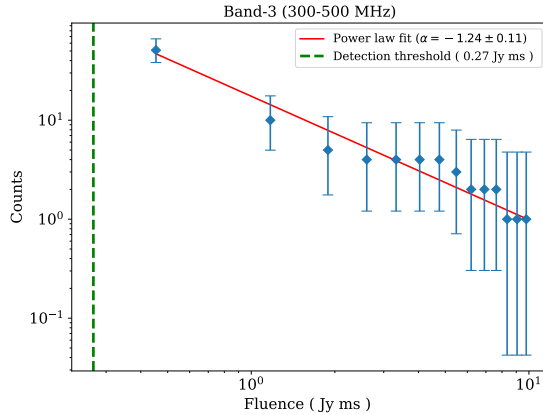


Figure 3. Cumulative distribution of the fluences of the bursts detected at band-3 (300-500 MHz). The green dashed line indicates the fluence threshold for a 2 ms burst detected at a S/N of 10. The red line indicates the fitted power-law.

series dedispersed at the detection DM (i.e., the DM which maximizes the S/N). We extract the time series around the burst’s arrival time and normalize the time series in units of the root mean square (RMS) noise measured from off-pulse. The time series is then calibrated to Jy units using the radiometer equation. To obtain the fluence for each burst, we sum the calibrated time series around the pulse region. After measuring the fluence for each pulse, we characterize the rate function of FRB 20240114A at 400 MHz. Figure 3 shows the log N - log S plot. We fit a power law using the optimization function `scipy.optimize.minimize`, taking into account Poissonian errors as described by (Cash 1979). All bursts have fluences below 10 Jy ms, suggesting that we are probing the lower end of the energy distribution. However, there have also been bright burst reported with fluences in excess of 10 Jy ms at P-band (Ould-Boukattine et al. 2024b; Pellicciari et al. 2024b). We do not include fluences measured for 5 bursts detected in band-4 since they were detected in IA beam.

To measure the pulse widths, we use the `scipy` module `curve_fit` to fit a Gaussian profile to each of the burst (component). The pulse widths range from 0.6 ms to 17 ms. The median pulse width of FRB 20240114A at 400 MHz is 4.3 ms, which is broader compared to 1.4 ms at 650 MHz (Panda et al. 2024b). The median for the SNR-optimised DM is 528.1 pc cm^{-3} .

3.2. Emission bandwidths

To characterize the emission bandwidth, we first down-sample the data from 1024 to 128 frequency channels and then average along the time axis around the burst region to estimate the average burst spectrum, as illustrated in the right panel of Figure 2. The average spectrum is the fitted with a Gaussian function

to estimate the peak frequency as well as the emission bandwidth (full width at half maximum). Most of the bursts exhibit narrow-band emission, as also apparent in Figure 1.

In Figure 2, two major trends are apparent. First, the peak emission frequency seems to decrease (roughly from 480 to 440 MHz) as the emission bandwidth increases from about 20 to 60 MHz. It is most likely caused by the band-edge and search sensitivity effects — near the top band-edge, we might be seeing only parts of the burst emission otherwise continuing outside our observing bandwidth. A similar but inverted trend would be expected at the lower edge of the band, and we see some hints of it. However, several parts of the spectrum in the lower half of the band (300-400 MHz) are typically contaminated by RFI, which effectively degrade the sensitivity in this part of the band. Consequently, we see this inverted trend effectively starting from roughly around the middle of the band. The distribution of the peak frequencies peaking around 450 MHz is also a consequence of the above band-edge effects. Figure 2 demonstrates that the emission is narrow-band for nearly all the bursts. The fractional bandwidth distribution peaks around 0.12.

3.3. Frequency drift rates

The sad-trombone effect or the downward-drifting pattern, is characteristic of repeating FRBs, with different repeating FRBs showing a wide variety of drift rates ranging from -1 to -60 MHz/ms (Pleunis et al. 2021b). Many of the bursts exhibit this downward drifting with single and multiple sub-bursts. The drift rates are typically estimated by first determining the structure-optimized DM and then exploiting 2-dimensional correlation. Due to the low S/N of our bursts, we could not utilise `DM_phase`³ (Seymour et al. 2019) for determining the structure optimized DM. We also could not use `frbgui`⁴ (Chamma et al. 2023) for the same reason. So, we use the S/N optimized DM to measure the relative TOAs and the central frequencies of the successive components in multi-component bursts to estimate the drift rate. The peak frequency of the sub-bursts are estimated as described in Section 3.2. The relative TOAs are determined by fitting a Gaussian function to each component in the band-averaged time profile. There are three bursts for which we could measure drift rates. One example of a burst for which we measured the drift rate is shown in right panel in Figure 4. The drift rate for this burst is estimated to be -0.35 ± 0.07 MHz/ms.

³ https://github.com/danielemichilli/DM_phase

⁴ <https://github.com/mef51/frbgui>

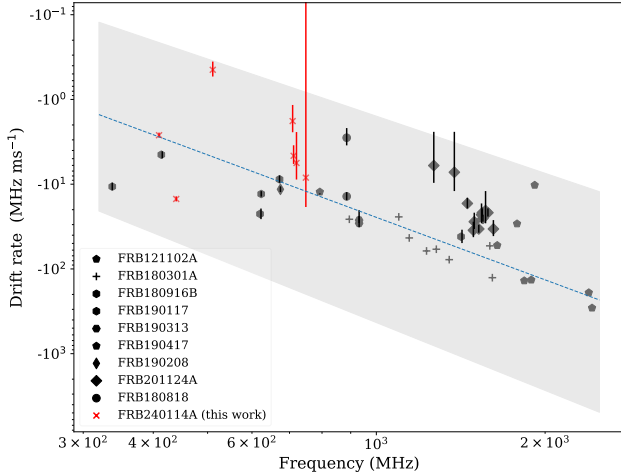


Figure 4. Drift rates as function of frequency, with both the quantities in the rest frame of the respective host galaxy, for FRB 20240114A and other repeaters (e.g. FRB121102A, FRB180916B). The dashed blue line and the region shaded around it indicate the power-law fit with its uncertainty, fitted by (Wang et al. 2022). References for measurements on other FRBs: Zhou et al. (2022); Kumar et al. (2023); CHIME/FRB Collaboration et al. (2019); Hessels et al. (2019); Pastor-Marazuela et al. (2021b); Marthi et al. (2020).

For the other bursts, the drift rate is estimated to be -11.7 ± 0.8 MHz/ms and -2.07 ± 0.14 MHz/ms. These measurements are comparable to the drift rates obtained for other repeaters at similar frequencies, as shown in Figure 4.

Using the data made publicly available by Panda et al. (2024b), we also measure drift rates for 4 bursts detected at band-4 which show well-separated, drifting components. The arrival times of the components are provided by the authors and we estimate the corresponding peak frequencies visually. We liberally assign large uncertainties to these visual estimates of peak frequencies, which often cover at least half of the total emission bandwidth for the respective components. The drift rates thus estimated are also shown in Figure 4.

4. IMAGING ANALYSIS AND RESULTS

Our observations in February and early March (at band-3 as well as band-4) often utilised recording the interferometric visibilities at 0.67 s integration time with the aim to localize the source to arcsecond precision (the position uncertainty at that time was about 1.5 arcmin Shin & CHIME/FRB Collaboration 2024). However, these observation did not result in detection of a burst with adequately high S/N for such a localization. Once the source was localized to arcsec precision by (Tian et al. 2024), our remaining observations (on 5, 8 and 24 March 2024) in band-3, used the new position as the

pointing center with an integration time of 10.7 s. For band 3 observations, we used 3C48 as the flux calibrator, and for band 4, we used 3C147 and 3C48 in different sessions, and with J2130+050 as the phase calibrator in all the observations. We used CAPTURE⁵ (Kale & Ishwara-Chandra 2021) for RFI flagging and calibration of the data.

After calibrating the data, we use CASA task `tclean` for imaging, with the deconvolution algorithm set to MTMFS and the Briggs weighting scheme (`robust = 0`). Self-calibration was performed until convergence to an image was achieved. We used `uGMRTprimarybeam` for primary beam correction for the band-4 image obtained from the 01 Feb 2024 session, since our pointing was slightly offset from the source position. From this observation, we place an upper limit of $140 \mu\text{Jy}$ (at 5σ level) on any continuum emission associated with the FRB (Kumar et al. 2024). From our more recent observation on 15 June 2024, we place the most stringent 5σ upper limit of $89 \mu\text{Jy}$ for continuum emission from any associated PRS or the host galaxy at 650 MHz (Panda et al. 2024b, placed a 5σ upper limit of $124 \mu\text{Jy}$ at the same frequency). Similarly, at band-3, we obtained the final images individually for the datasets from 5, 8, and 24 March observations. In the best image, we do not detect any continuum emission up to $600 \mu\text{Jy}$ (at 5σ level) with an on-source time of 78 minutes. We note that there is a bright (325 mJy) source between the FWHM and first null of the uGMRT primary beam. Thus, deconvolution errors limits the RMS noise achievable for the band-3 image despite the longer on-source time. We provide the upper limits for spectral luminosity at 650 MHz and 400 MHz using the redshift of 0.13 (Bhardwaj et al. 2024). We also obtain image in band-5 with on source time of 65 min but the observations were heavily affected by RFI. Nevertheless, we provide an upper limit of 1 mJy for the PRS at 1.26 GHz using these band-5 data. Figure 5⁶ shows the comparison of our upper limits on emission from a persistent radio source (PRS) associated with FRB 20240114A, along with that for PRSs associated with FRB121102A and FRB190520B, and upper limits on similar emission from various repeating and non-repeating FRBs, as well as SGR 1935+2154.

5. DISCUSSION

Our efforts to understand the nature of FRB 20240114A included a prompt follow-up in February and March 2024, at band-3 as well as band-4 of uGMRT right after its discovery. From the observation on 1 February

⁵ <https://github.com/ruta-k/CAPTURE-CASA6>

⁶ $L\nu$ is calculated assuming a flat spectrum.

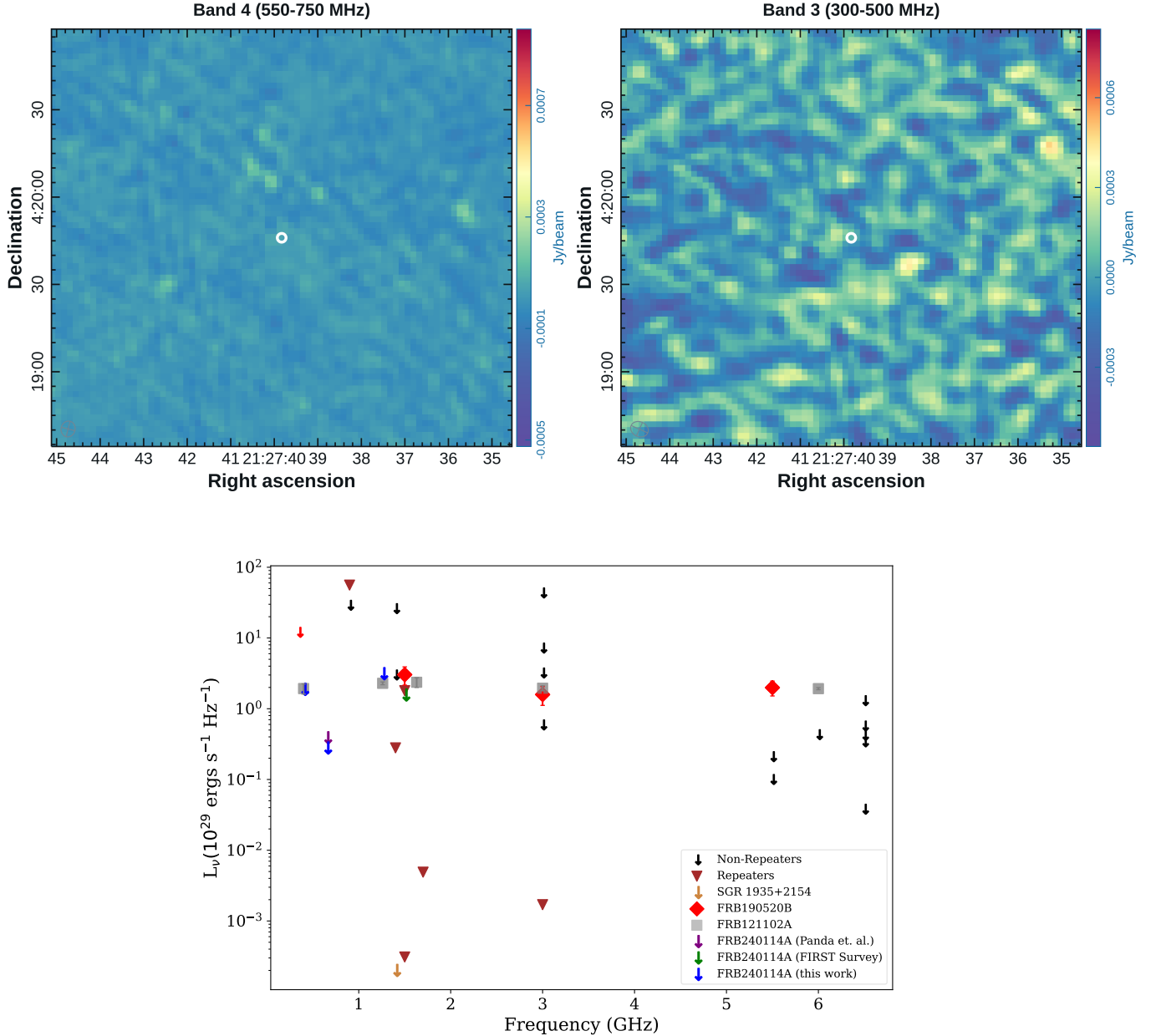


Figure 5. *Top:* Images of the sky regions around the sky-position of FRB 20240114A, at 650 MHz and 400 MHz. The MeerKAT localisation of FRB 20240114A is marked with a circle at the center of the images. *Bottom:* Comparison of upper limits and measurements of spectral luminosity of PRS, associated with repeating and non-repeating FRBs, and SGR 1935+2154, along with our upper limits for FRB 20240114A at different frequencies. References: Law et al. (2022); Resmi, L. et al. (2021); Chatterjee et al. (2017b); Zhang et al. (2023); Niu et al. (2022). For the original references for upper limits on various repeaters, non-repeating FRBs and SGR 1935+2154, please see Law et al. (2022).

at band-4, we detected bursts in the IA beam but not in the PA beam, suggesting that the position reported by CHIME was offset from the actual source position by at least 1.1 arcmin (i.e., half-power beam width), a finding later confirmed by the MeerKAT localization (Tian et al. 2024). Subsequent observations in band-3 and band-5 also did not result in bursts adequately bright enough to localize the source. In these early ob-

servations, we detected five bursts in Band-3 in the PA beam (but not in the IA beam, as these were all faint bursts), and none at band-5. With these detections, we confirmed the high activity phase of FRB 20240114A in the 300-750 MHz frequency range (Kumar et al. 2024). Using the subsequent observations in March, now with adequately precise position estimate from MeerKAT, we measure significant variations in the activity levels of

FRB 20240114A which could be related to the underlying emission mechanism or propagation effects. While a few repeating FRBs show periodic modulation in their activity (Chime/Frb Collaboration et al. 2020; Rajwade et al. 2020b), a few others show high activity phases (e.g., burst storms) followed by a long quiescence (Lanman et al. 2022). Currently there is no clear picture what causes such modulations, periodic or otherwise, in the bursting activity.

5.1. Frequency-dependent activity

FRB 20240114A has been followed up by various telescopes at a variety of observing frequencies covering the range 0.3–6 GHz. We compiled a summary of these observations and burst detections reported by various groups through ATels and show it in Figure 1. Limited by the details provided in various ATels as well as for the convenience of displaying, we quantize the observing frequency into four ranges: 0.3-0.8, 0.8-2, 2-4, and 4-6 GHz. Similarly, the time span between the discovery and first week of May is divided into 10 parts. We note that at L-band and lower frequencies (i.e., the first two frequency ranges), bursts from FRB 20240114A have been detected regularly. However, at the frequencies higher than 2 GHz, bursts have been detected only in the later half of April and beginning of May, despite regular observations earlier too. So, there is an indication of a potential chromaticity in the activity, where FRB 20240114A is becoming active at higher frequencies at the later epochs. Non-detection of any burst from our latest band-4 observation on 29 May 2024 also indicate towards quenching of the burst activity at lower frequencies.

FRB 20180916B is the only FRB for which evidence of chromaticity in its activity has been seen (Pastor-Marazuela et al. 2021b; Pleumis et al. 2021c). Despite having only a moderate burst rate, the discovery of the chromaticity was aided by the knowledge of the underlying modulation period of the FRB 20180916B. For FRB 20240114A, an underlying periodicity, if any, in its activity is yet to be detected. Moreover, the frequency chromaticity in FRB 20240114A appears to be opposite to that in FRB 20180916B, i.e., the burst activity at higher frequencies seem to be delayed in FRB 20240114A while the opposite is true for FRB 20180916B.

We note that the currently available information on FRB 20240114A is not sufficient to establish or rule out above potential chromaticity. For example, bursts at in the 2–6 GHz frequency range have been detected by sensitive telescopes like Effelsberg and Nancay (Limaye & Spitler 2024; Hewitt et al. 2024; Joshi et al. 2024). However, the observations displayed for the 4–6 GHz

range in Figure 1 are mostly by much smaller telescopes and different setups, e.g., with smaller bandwidths (Ould-Boukattine et al. 2024b). Any lack of sub-band searches might also have contributed to the sensitivity differences. Furthermore, the narrow-band emission of the bursts combined with narrow observing bandwidths might also have been decisive. With a detailed information of various observing setups, it might be possible to conduct simulations to further probe if there is indeed chromaticity in the FRB 20240114A’s activity, however, that is beyond the scope of this work. Nevertheless, a systematic, multi-frequency monitoring of the source is needed to better probe this potential chromaticity as well as any underlying periodicity.

Furthermore, Zhang et al. (2024b) conducted observations on 28 and 29 January 2024, and 01 and 04 February 2024, detecting 38 bursts with a total on-source time of 2 hours. The inferred burst rate at approximately 1.1 GHz is 20 hr^{-1} above the fluence threshold of around 0.015 Jy ms. Assuming a mean power law index of -1.5, the burst rate would be only 0.072 hr^{-1} at a fluence threshold of 0.64 Jy ms. However, we estimate the burst rate to be 2.6 hr^{-1} at 400 MHz from our first band-3 observation on 08 February 2024, indicating a sharp evolution of burst rate with observing frequency and/or time.

5.2. Spectro-temporal Properties

The width distribution (not shown but assessed separately) of the bursts we detected shows a median width of 4.3 ms at 400 MHz which is larger than the median width of 1.4 ms reported at 650 MHz (Panda et al. 2024b). In the left panel in Figure 2, we see that the peak frequency of majority of the bursts is above 400 MHz, potentially suggesting a preference for the emission frequencies to be above 400 MHz. However, there could also be detection biases, e.g., lower sensitivity in the lower half of band-3 due to presence of RFI and scatter broadening. Most of the bursts in our sample show narrow-band emission. Similar behavior has been observed at 600 MHz with CHIME and at L-band with FAST (Zhang et al. 2024b; Shin & CHIME/FRB Collaboration 2024). Narrow-band emission has also been observed in the giant pulses of the Crab pulsar and FRB 20190711A (Thulasiram & Lin 2021; Kumar et al. 2021b) with similar values of $\Delta\nu/\nu$ as for FRB 20240114A. There is the possibility of bursts being narrow due to emission being below our detection threshold at other frequencies and brightest at frequencies where we detect them, which effectively implies steep modulations in the burst spectra. Cordes et al. (2017) shows that caustics can produce strong magnifications ($\leq 10^2$) in plasma and present as spectral peaks in the frequency

range 0.1-1 GHz. Plasma lensing has been invoked to explain narrow-band and high-energy bursts for repeating FRBs, e.g., FRB121102A, FRB201124A (Chen et al. 2024). Metzger et al. (2019) invokes synchrotron maser emission in ultra-relativistic magnetized shocks to produce the downward drifting pattern. Under certain conditions, it predicts a simultaneous narrow-band emission that is not intrinsic but most likely caused by the propagation effects, e.g. plasma lensing.

Wang et al. (2022) modeled the drift rates of various repeating FRBs as a function of frequency (in the rest frame of the host galaxy) with a power-law. They suggest that the downward drift can be explained through curvature radiation in magnetars originating from different heights. Figure 4 shows that the drift rates we measured for FRB 20240114A also agree with the relationship modeled by Wang et al. (2022). In the lower frequency regime, FRB180916B has been the only other FRB with such measurements. Our measurements for FRB 20240114A further populate this part of the phase space.

5.3. Energetics

Several bursts have now been reported from FRB 20240114A that have fluence in excess of 50 Jy ms (Ould-Boukattine et al. 2024a; Pellicciari et al. 2024b; Ould-Boukattine et al. 2024b; Shin & CHIME/FRB Collaboration 2024), however, all the bursts except one we detected have fluences below 10 Jy ms (twice of the CHIME/FRB’s typical detection threshold). This might suggest that most of the time the source might be emitting relatively low energy bursts, also seen by Zhang et al. (2024b), and high energy bursts might be following a different mean burst rate and power-law statistics. If this is really the case, it would remain to be seen whether the two population of bursts are caused by different emission mechanisms or propagation effects (e.g., plasma lensing). Particularly for FRB20201124A, Kirsten et al. (2023) argue that the higher energy burst population cannot be explained by lensing effects and the increased brightness is intrinsic.

For FRB 20240114A, We obtain a power-law index of -1.24 ± 0.11 for the bursts we detected at 400MHz. We note that, much like several other works following the same approach, our fluences are estimated from the band-averaged bursts, even for the bursts clearly having narrow bandwidths. Our measured power-law index of -1.24 ± 0.11 reconciles with that for several other repeaters for which a wide range from relatively flat index of -0.5 to as steep as -4.9 has been reported (Kirsten et al. 2023). This index also varies with time and the range of observed energies of the bursts (Kirsten et al.

2023). For FRB 20240114A, Panda et al. (2024b) fit a broken power law for bursts detected at 650 MHz with index at lower end to be -0.7 which is flatter than what we measure at 400 MHz. While this could suggest a dynamic or frequency-dependent change in the energy distribution, it could also result from incompleteness in search for lower fluence bursts.

A similar power-law index has been seen for several other repeating FRBs as well as the giant pulses from the Crab pulsar and the magnetar XTE 1810–197 (Maan et al. 2019b; Serylak et al. 2009). However, different measurements have resulted into different power-law indices for the same sources, indicating temporal evolution or a more complex distribution of the bursts.

5.4. Persistent Radio Source

Persistent radio sources (PRS) have been associated with two repeating FRBs so far, FRB 20190520B and FRB 20121124A (Chatterjee et al. 2017b; Niu et al. 2022). For both FRBs, we see that there is temporal evolution of the associated PRS flux densities (Rhodes et al. 2023; Chen et al. 2023). Figure 5 shows the spectral luminosity of the PRS associated with the above two repeating FRBs at different frequencies, along with the upper limits for a few repeating and one-off FRBs as well as our upper limits on the spectral luminosity of any PRS associated with FRB 20240114A at 400 and 650 MHz. Specially at 650 MHz, our upper limit is almost an order of magnitude below the spectral luminosity of the two known PRS.

Two models have been invoked to explain the persistent radio emission — one involves magnetized ion-electron nebula (Margalit & Metzger 2018) and other involves a hypernebulula i.e hyperaccreting compact object (Sridhar & Metzger 2022). While our limits are quite stringent at lower frequencies, a spectral turn-over around or above 1 GHz can not be ruled out. In that case, it might still be possible to detect the PRS at higher frequencies. Furthermore, the turn-over is expected to shift to lower radio frequencies with time (Margalit & Metzger 2018), and hence the PRS could also become detectable even at 650 MHz at a later epoch. In such a case, our current limits would be useful in constraining the temporal evolution. Overall, a regular sensitive observations at a few different frequencies would be useful to probe any associated PRS.

Law et al. (2022) studied any potential correlations between various burst properties, e.g., the repetition rate, and the associated PRS luminosity. An interesting idea is that the excess DM caused by the host galaxy, DM_{host} , might be causally connected to the PRS (Law et al. 2022). For FRB 20240114A, DM_{host} could be around

330pc cm^{-3} (Bhardwaj et al. 2024), which is larger than the typical contribution from the ISM in the host galaxies. When compared to the DM_{host} and repetition rate of FRBs with and without an associated PRS, FRB 20240114A’s DM_{host} and repetition rate might favor the presence of a PRS. However, DM_{host} normalized by the stellar mass of the galaxy could be more informative (Law et al. 2022, e.g., their figure 4).

6. CONCLUSIONS

We report detection of 57 bursts from FRB 20240114A at band-3 (300-500 MHz) and band-4 (550-750 MHz) of uGMRT. We also confirm the lower frequency counterpart of the burst storm that was reported at L-band with a rate of 500 hr^{-1} using FAST on 5th Mar 2024, but with a bursts rate of 31 hr^{-1} above a fluence threshold of 0.22 Jy ms for 2 ms wide bursts at 400 MHz. From a detailed analysis of our low-energy burst sample as well as considering the reported detection of FRB 20240114A from other telescopes, we conclude the following.

1. The fluence distribution of the FRB 20240114A bursts at 400 MHz in the range 0.1–10 Jy ms is well fit with a single power-law index of -1.24 ± 0.11 .
2. The bursts from FRB 20240114A exhibit narrow-band (about 10% fractional bandwidth) behaviour and downward drifting pattern similar to many other repeating FRBs. Our drift-rate estimates for FRB 20240114A are such measurements at the second lowest frequency for any FRB so far. The drift rates are consistent with the power-law fit for such estimates from various FRBs at their rest frame frequencies, and might indicate curvature radiation at different heights as the origin of the observed downward drifting emission.
3. We place the most stringent upper limits at 400 and 650 MHz on the spectral luminosity of any underlying PRS associated with FRB 20240114A. The upper limit at 650 MHz is nearly an order of magnitude below the luminosity of the two known PRS at this frequency. However, a spectral

turnover at higher frequencies can not be ruled out as the cause of the non-detection, and continued monitoring would be helpful.

4. Finally, FRB 20240114A shows frequency dependent burst rate. By combining the information available from follow-ups at other telescopes and frequencies, we also show that the burst activity of FRB 20240114A is potentially frequency dependent. Our latest observation at band-4 also indicate towards a potential quenching of the activity at low frequencies.

Overall, the similarity of various properties of FRB 20240114A to other repeating FRBs suggest a common intrinsic nature of emission. Our results also warrant for a multi-frequency monitoring of FRB 20240114A to establish the potential frequency dependent activity and probe a spectral turn-over evolution of any associated PRS.

7. SOFTWARE AND THIRD PARTY DATA REPOSITORY CITATIONS

Facilities: Giant Meterwave Radio Telescope, Khodad, Pune

Software: astropy (Astropy Collaboration et al. 2013), matplotlib (Hunter 2007), scipy (Virtanen et al. 2020), your (Aggarwal et al. 2020), RFIClean (Maan et al. 2021), PRESTO (Ransom 2011)

ACKNOWLEDGMENTS

YM acknowledges support from the Department of Science and Technology via the Science and Engineering Research Board Startup Research Grant (SRG/2023/002657). We would like to thank Ramananda Santra for useful discussions regarding interferometric data analysis. AK would like to thank Arvind Balasubramanian for useful discussions. We would like to thank the Centre Director and the observatory for the prompt time-allocation and scheduling of our observations. GMRT is run by the National Centre for Radio Astrophysics of the Tata Institute of Fundamental Research.

REFERENCES

- Aggarwal, K., Agarwal, D., Kania, J. W., et al. 2020, Journal of Open Source Software, 5, 2750, doi: 10.21105/joss.02750
- Astropy Collaboration, Robitaille, T. P., Tollerud, E. J., et al. 2013, A&A, 558, A33, doi: 10.1051/0004-6361/201322068

- Bannister, K. W., Deller, A. T., Phillips, C., et al. 2019, *Science*, 365, 565, doi: [10.1126/science.aaw5903](https://doi.org/10.1126/science.aaw5903)
- Bhandari, S., Sadler, E. M., Prochaska, J. X., et al. 2020, *ApJL*, 895, L37, doi: [10.3847/2041-8213/ab672e](https://doi.org/10.3847/2041-8213/ab672e)
- Bhardwaj, M., Kirichenko, A., & Gil de Paz, A. 2024, *The Astronomer's Telegram*, 16613, 1
- Bochenek, C. D., Ravi, V., Belov, K. V., et al. 2020, *Nature*, 587, 59, doi: [10.1038/s41586-020-2872-x](https://doi.org/10.1038/s41586-020-2872-x)
- Cash, W. 1979, *ApJ*, 228, 939, doi: [10.1086/156922](https://doi.org/10.1086/156922)
- Chamma, M. A., Rajabi, F., Kumar, A., & Houde, M. 2023, *Monthly Notices of the Royal Astronomical Society*, 522, 3036–3048, doi: [10.1093/mnras/stad1108](https://doi.org/10.1093/mnras/stad1108)
- Chatterjee, S., Law, C. J., Wharton, R. S., et al. 2017a, *Nature*, 541, 58, doi: [10.1038/nature20797](https://doi.org/10.1038/nature20797)
- . 2017b, *Nature*, 541, 58, doi: [10.1038/nature20797](https://doi.org/10.1038/nature20797)
- Chen, G., Ravi, V., & Hallinan, G. W. 2023, *The Astrophysical Journal*, 958, 185, doi: [10.3847/1538-4357/ad02f3](https://doi.org/10.3847/1538-4357/ad02f3)
- Chen, X., Hu, B., Wang, P., et al. 2024, Plasma lensing interpretation of FRB 20201124A bursts at the end of September 2021. <https://arxiv.org/abs/2401.18036>
- CHIME/FRB Collaboration, Andersen, B. C., Bandura, K., et al. 2019, *ApJL*, 885, L24, doi: [10.3847/2041-8213/ab4a80](https://doi.org/10.3847/2041-8213/ab4a80)
- Chime/Frb Collaboration, Amiri, M., Andersen, B. C., et al. 2020, *Nature*, 582, 351, doi: [10.1038/s41586-020-2398-2](https://doi.org/10.1038/s41586-020-2398-2)
- CHIME/FRB Collaboration, Andersen, B. C., Bandura, K. M., et al. 2020, *Nature*, 587, 54, doi: [10.1038/s41586-020-2863-y](https://doi.org/10.1038/s41586-020-2863-y)
- Chime/Frb Collaboration, Amiri, M., Andersen, B. C., et al. 2020, *Nature*, 582, 351, doi: [10.1038/s41586-020-2398-2](https://doi.org/10.1038/s41586-020-2398-2)
- Cordes, J. M., Wasserman, I., Hessels, J. W. T., et al. 2017, *ApJ*, 842, 35, doi: [10.3847/1538-4357/aa74da](https://doi.org/10.3847/1538-4357/aa74da)
- Feng, Y., Li, D., Zhang, Y.-K., et al. 2023, arXiv e-prints, arXiv:2304.14671, doi: [10.48550/arXiv.2304.14671](https://doi.org/10.48550/arXiv.2304.14671)
- Gopinath, A., Bassa, C. G., Pleunis, Z., et al. 2023, *Monthly Notices of the Royal Astronomical Society*, 527, 9872, doi: [10.1093/mnras/stad3856](https://doi.org/10.1093/mnras/stad3856)
- Gupta, Y., Ajithkumar, B., Kale, H. S., et al. 2017, *Current Science*, 113, 707, doi: [10.18520/cs/v113/i04/707-714](https://doi.org/10.18520/cs/v113/i04/707-714)
- Heintz, K. E., Prochaska, J. X., Simha, S., et al. 2020, *ApJ*, 903, 152, doi: [10.3847/1538-4357/abb6fb](https://doi.org/10.3847/1538-4357/abb6fb)
- Hessels, J. W. T., Spitler, L. G., Seymour, A. D., et al. 2019, *ApJL*, 876, L23, doi: [10.3847/2041-8213/ab13ae](https://doi.org/10.3847/2041-8213/ab13ae)
- Hewitt, D. M., Huang, J., Hessels, J. W. T., et al. 2024, *The Astronomer's Telegram*, 16597, 1
- Hunter, J. D. 2007, *Computing in Science & Engineering*, 9, 90, doi: [10.1109/MCSE.2007.55](https://doi.org/10.1109/MCSE.2007.55)
- Joshi, P., Medina, A., Earwicker, J. T., et al. 2024, *The Astronomer's Telegram*, 16599, 1
- Kale, R., & Ishwara-Chandra, C. H. 2021, *Experimental Astronomy*, 51, 95, doi: [10.1007/s10686-020-09677-6](https://doi.org/10.1007/s10686-020-09677-6)
- Kirsten, F., Ould-Boukattine, O., Herrmann, W., et al. 2023, Connecting repeating and non-repeating fast radio bursts via their energy distributions. <https://arxiv.org/abs/2306.15505>
- Kumar, A., Maan, Y., & Bhusare, Y. 2024, *The Astronomer's Telegram*, 16452, 1
- Kumar, P., Shannon, R. M., Flynn, C., et al. 2021a, *MNRAS*, 500, 2525, doi: [10.1093/mnras/staa3436](https://doi.org/10.1093/mnras/staa3436)
- . 2021b, *MNRAS*, 500, 2525, doi: [10.1093/mnras/staa3436](https://doi.org/10.1093/mnras/staa3436)
- Kumar, P., Luo, R., Price, D. C., et al. 2023, *MNRAS*, 526, 3652, doi: [10.1093/mnras/stad2969](https://doi.org/10.1093/mnras/stad2969)
- Lanman, A. E., Andersen, B. C., Chawla, P., et al. 2022, *The Astrophysical Journal*, 927, 59
- Law, C. J., Connor, L., & Aggarwal, K. 2022, *ApJ*, 927, 55, doi: [10.3847/1538-4357/ac4c42](https://doi.org/10.3847/1538-4357/ac4c42)
- Limaye, P., & Spitler, L. 2024, *The Astronomer's Telegram*, 16620, 1
- Maan, Y., Joshi, B. C., Surnis, M. P., Bagchi, M., & Manoharan, P. K. 2019a, *ApJL*, 882, L9, doi: [10.3847/2041-8213/ab3a47](https://doi.org/10.3847/2041-8213/ab3a47)
- . 2019b, *ApJL*, 882, L9, doi: [10.3847/2041-8213/ab3a47](https://doi.org/10.3847/2041-8213/ab3a47)
- Maan, Y., van Leeuwen, J., & Vohl, D. 2021, *Astronomy & Astrophysics*, 650, A80, doi: [10.1051/0004-6361/202040164](https://doi.org/10.1051/0004-6361/202040164)
- Marcote, B., Nimmo, K., Hessels, J. W. T., et al. 2020, *Nature*, 577, 190, doi: [10.1038/s41586-019-1866-z](https://doi.org/10.1038/s41586-019-1866-z)
- Margalit, B., & Metzger, B. D. 2018, *The Astrophysical Journal Letters*, 868, L4, doi: [10.3847/2041-8213/aaedad](https://doi.org/10.3847/2041-8213/aaedad)
- Marthi, V. R., Gautam, T., Li, D. Z., et al. 2020, *MNRAS*, 499, L16, doi: [10.1093/mnras/slaa148](https://doi.org/10.1093/mnras/slaa148)
- Metzger, B. D., Margalit, B., & Sironi, L. 2019, *MNRAS*, 485, 4091, doi: [10.1093/mnras/stz700](https://doi.org/10.1093/mnras/stz700)
- Niu, C. H., Aggarwal, K., Li, D., et al. 2022, *Nature*, 606, 873, doi: [10.1038/s41586-022-04755-5](https://doi.org/10.1038/s41586-022-04755-5)
- Ould-Boukattine, O. S., Hessels, J. W. T., Kirsten, F., et al. 2024a, *The Astronomer's Telegram*, 16432, 1
- Ould-Boukattine, O. S., Dijkema, T. J., Gawronski, M., et al. 2024b, *The Astronomer's Telegram*, 16565, 1
- Panda, U., Bhattacharyya, S., Dudeja, C., Kudale, S., & Roy, J. 2024a, *The Astronomer's Telegram*, 16494, 1
- Panda, U., Roy, J., Bhattacharyya, S., Dudeja, C., & Kudale, S. 2024b, arXiv e-prints, arXiv:2405.09749, doi: [10.48550/arXiv.2405.09749](https://doi.org/10.48550/arXiv.2405.09749)
- Pastor-Marazuela, I., Connor, L., van Leeuwen, J., et al. 2021a, *Nature*, 596, 505, doi: [10.1038/s41586-021-03724-8](https://doi.org/10.1038/s41586-021-03724-8)

- . 2021b, *Nature*, 596, 505, doi: [10.1038/s41586-021-03724-8](https://doi.org/10.1038/s41586-021-03724-8)
- Pellicciari, D., Geminardi, A., Bernardi, G., et al. 2024a, *The Astronomer's Telegram*, 16434, 1
- . 2024b, *The Astronomer's Telegram*, 16547, 1
- Pleunis, Z., Michilli, D., Bassa, C. G., et al. 2021a, *ApJL*, 911, L3, doi: [10.3847/2041-8213/abec72](https://doi.org/10.3847/2041-8213/abec72)
- Pleunis, Z., Good, D. C., Kaspi, V. M., et al. 2021b, *ApJ*, 923, 1, doi: [10.3847/1538-4357/ac33ac](https://doi.org/10.3847/1538-4357/ac33ac)
- Pleunis, Z., Michilli, D., Bassa, C. G., et al. 2021c, *ApJL*, 911, L3, doi: [10.3847/2041-8213/abec72](https://doi.org/10.3847/2041-8213/abec72)
- Rajwade, K. M., Mickaliger, M. B., Stappers, B. W., et al. 2020a, *MNRAS*, 495, 3551, doi: [10.1093/mnras/staa1237](https://doi.org/10.1093/mnras/staa1237)
- . 2020b, *MNRAS*, 495, 3551, doi: [10.1093/mnras/staa1237](https://doi.org/10.1093/mnras/staa1237)
- Ransom, S. 2011, PRESTO: Pulsar Exploration and Search TOolkit, Astrophysics Source Code Library, record ascl:1107.017
- Resmi, L., Vink, J., & Ishwara-Chandra, C. H. 2021, *A&A*, 655, A102, doi: [10.1051/0004-6361/202039771](https://doi.org/10.1051/0004-6361/202039771)
- Rhodes, L., Caleb, M., Stappers, B. W., et al. 2023, *MNRAS*, 525, 3626, doi: [10.1093/mnras/stad2438](https://doi.org/10.1093/mnras/stad2438)
- Serylak, M., Stappers, B. W., Weltevrede, P., et al. 2009, *MNRAS*, 394, 295, doi: [10.1111/j.1365-2966.2008.14260.x](https://doi.org/10.1111/j.1365-2966.2008.14260.x)
- Seymour, A., Michilli, D., & Pleunis, Z. 2019, DM_phase: Algorithm for correcting dispersion of radio signals, Astrophysics Source Code Library, record ascl:1910.004
- Shin, K., & CHIME/FRB Collaboration. 2024, *The Astronomer's Telegram*, 16420, 1
- Snelders, M. P., Bhandari, S., Kirsten, F., et al. 2024, *The Astronomer's Telegram*, 16542, 1
- Spitler, L. G., Cordes, J. M., Hessels, J. W. T., et al. 2014, *ApJ*, 790, 101, doi: [10.1088/0004-637X/790/2/101](https://doi.org/10.1088/0004-637X/790/2/101)
- Sridhar, N., & Metzger, B. D. 2022, *ApJ*, 937, 5, doi: [10.3847/1538-4357/ac8a4a](https://doi.org/10.3847/1538-4357/ac8a4a)
- Thulasiram, P., & Lin, H.-H. 2021, *MNRAS*, 508, 1947, doi: [10.1093/mnras/stab2692](https://doi.org/10.1093/mnras/stab2692)
- Thulasiram, P., & Lin, H.-H. 2021, *Monthly Notices of the Royal Astronomical Society*, 508, doi: [10.1093/mnras/stab2692](https://doi.org/10.1093/mnras/stab2692)
- Tian, J., Pastor-Marazuela, I., Stappers, B., et al. 2024, *The Astronomer's Telegram*, 16446, 1
- Uttarkar, P. A., Kumar, P., Lower, M. E., & Shannon, R. M. 2024, *The Astronomer's Telegram*, 16430, 1
- Virtanen, P., Gommers, R., Oliphant, T. E., et al. 2020, *Nature Methods*, 17, 261, doi: [10.1038/s41592-019-0686-2](https://doi.org/10.1038/s41592-019-0686-2)
- Wang, W.-Y., Yang, Y.-P., Niu, C.-H., Xu, R., & Zhang, B. 2022, *ApJ*, 927, 105, doi: [10.3847/1538-4357/ac4097](https://doi.org/10.3847/1538-4357/ac4097)
- Zhang, J., Wu, Q., Cao, S., et al. 2024a, *The Astronomer's Telegram*, 16505, 1
- Zhang, J., Zhu, Y., Cao, S., et al. 2024b, *The Astronomer's Telegram*, 16433, 1
- Zhang, X., Yu, W., Law, C., et al. 2023, *ApJ*, 959, 89, doi: [10.3847/1538-4357/ad0545](https://doi.org/10.3847/1538-4357/ad0545)
- Zhou, D. J., Han, J. L., Zhang, B., et al. 2022, *Research in Astronomy and Astrophysics*, 22, 124001, doi: [10.1088/1674-4527/ac98f8](https://doi.org/10.1088/1674-4527/ac98f8)